Electronic supplementary information

Engineering Electronic Structure of 1T'-ReS_2 through Nitrogen Implantation for Enhanced Alkaline Hydrogen Evolution

Qiaozhi Sun,[a] Biao Zhang,[a] Lechen Diao,[a] Biao Chen,[a] Kai Song,[a] Liying Ma[*ab], and Fang He*[*ab]*

[a]School of Materials Science and Engineering and Tianjin Key Laboratory of Composites and Functional Materials, Tianjin University, Tianjin 300072, P. R. China.

[b]Collaborative Innovation Center of Chemical Science and Engineering, Tianjin 300072, China.

* Corresponding author. E-mail: fanghe@tju.edu.cn; lyma@tju.edu.cn

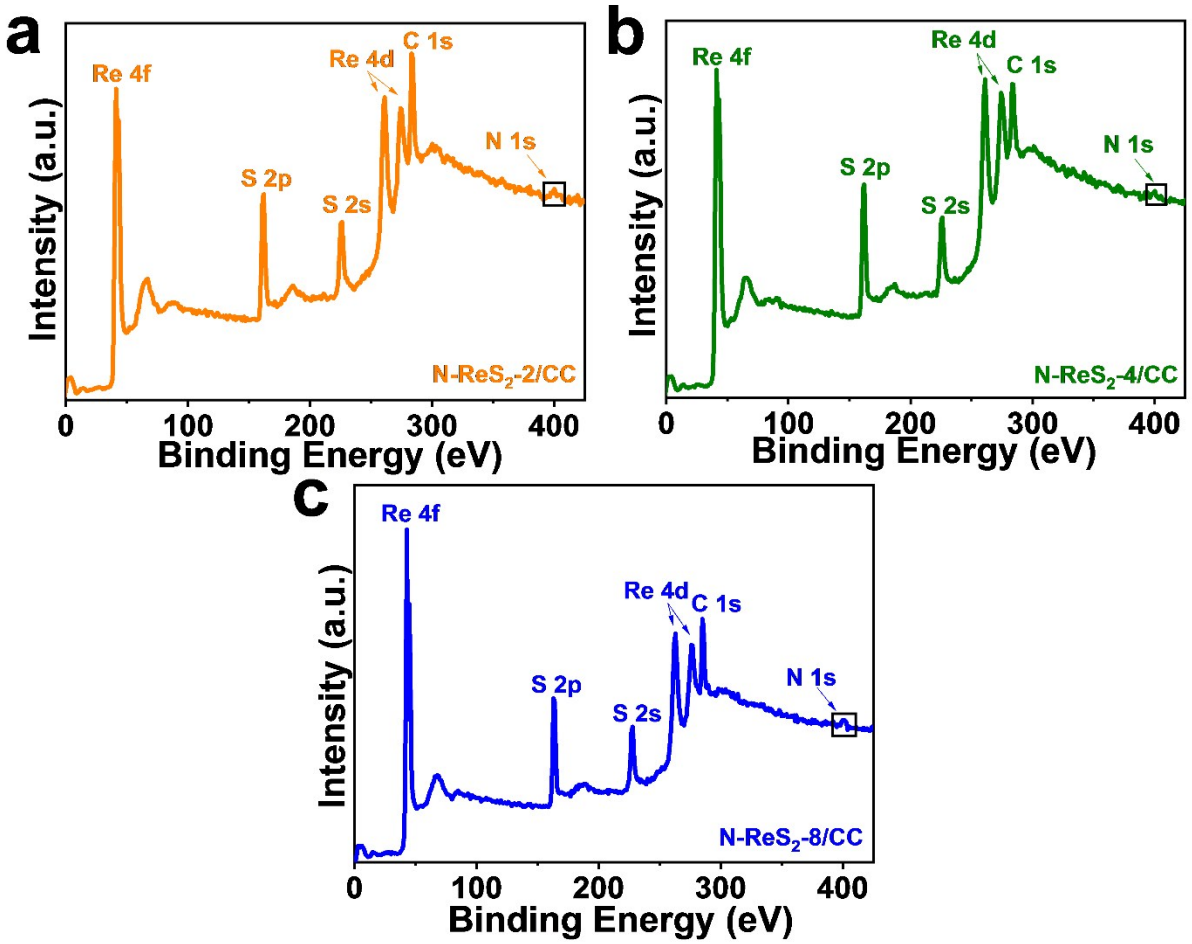

Fig. S1. XPS survey spectra of (a) N-ReS_2-2/CC, (b) N-ReS_2-4/CC and (c) N-ReS_2-8/CC.

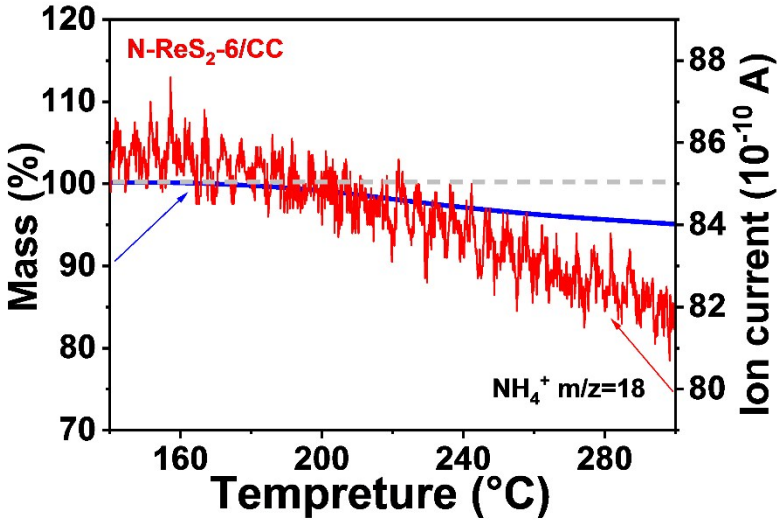

Fig. S2. TG-MS curve of N-ReS_2-6/CC.

The TG-MS curve shows no mass loss step corresponding to the release of NH_4^+ (c.a. 7.3 wt.%, m/z = 18) at c.a. 260 °C.[1]

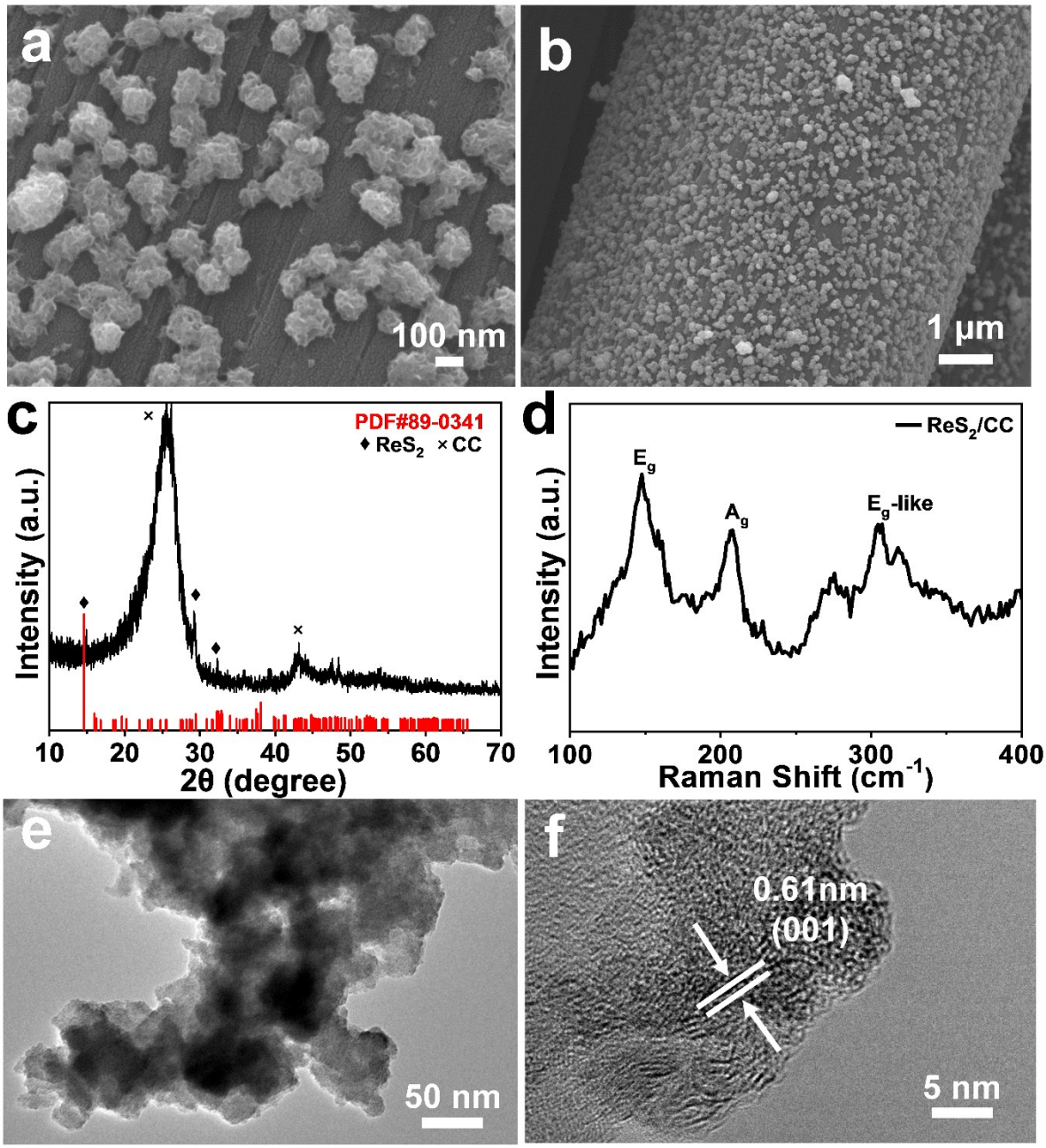

Fig. S3. (a, b) SEM images, (c) XRD pattern, (d) Raman spectrum, (e) TEM and (f) HRTEM images of ReS_2/CC.

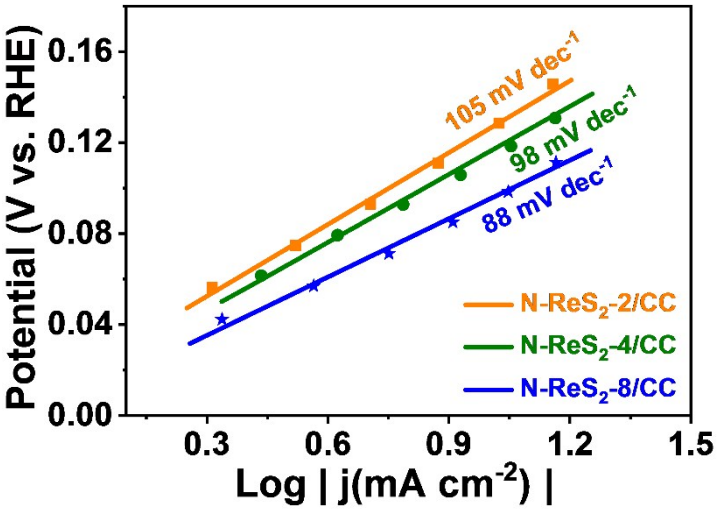

Fig. S4. Tafel plots of N-ReS_2-2/CC, N-ReS_2-4/CC and N-ReS_2-8/CC.

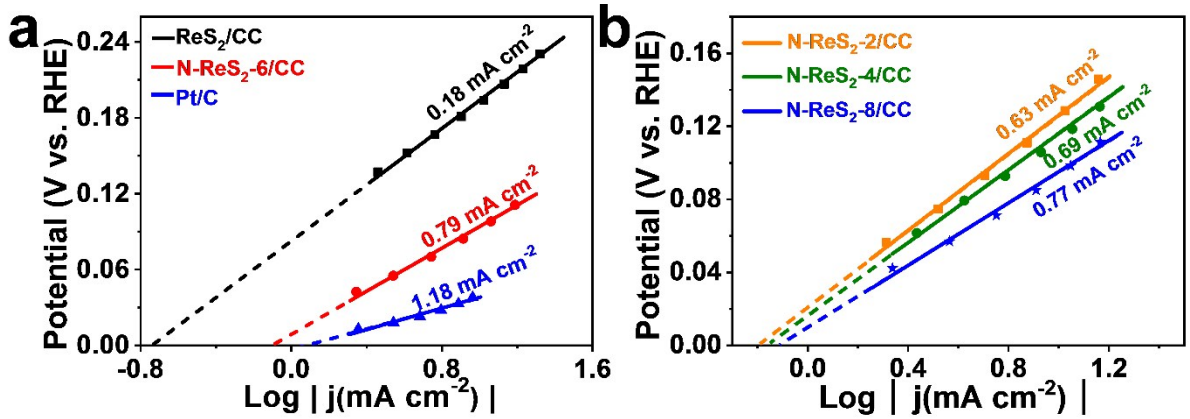

Fig. S5. (a, b) Tafel plots of catalysts. The exchange current density (j_0) is calculated from the Tafel plots by an extrapolation method according to the following equation: $\eta = a + b \log j$, where a is the intercept on the y-axis and b is Tafel slope. Exchange current density (j_0) is calculated when $\eta = 0$ V.

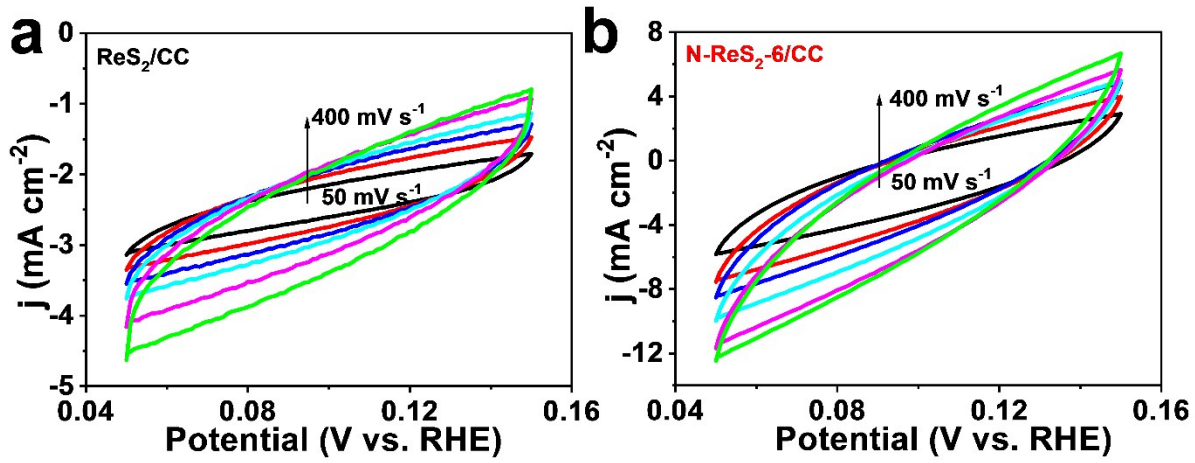

Fig. S6. CV curves of sample (a) ReS_2/CC and (b) N-ReS_2-6/CC in the region of 0.05-0.15 V vs. RHE.

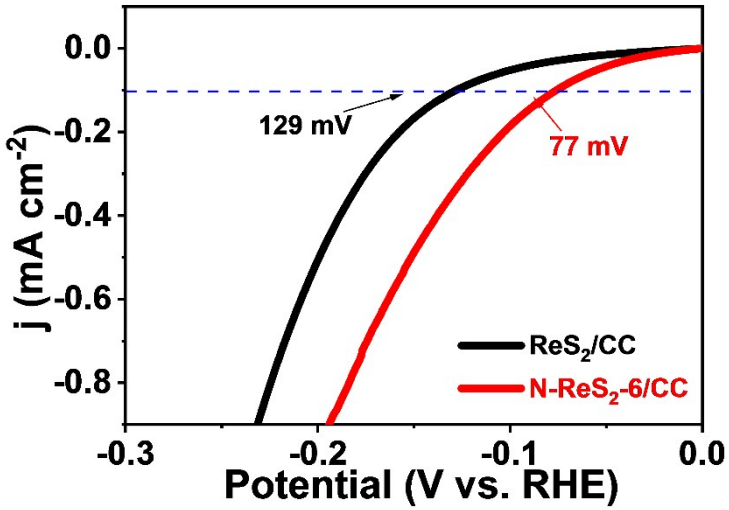

Fig. S7. LSV curves for HER with current density normalized by enlarged ECSA.

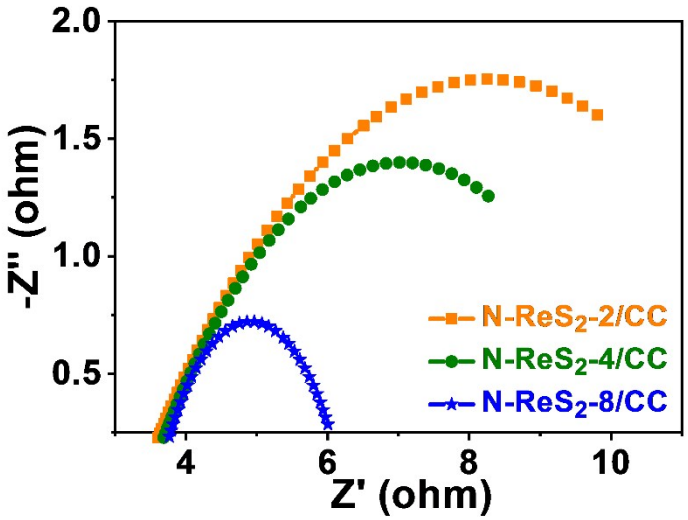

Fig. S8. Nyquist plots of N-ReS_2-2/CC, N-ReS_2-4/CC and N-ReS_2-8/CC.

The R_{ct} values are calculated to be 10, 7, and 3 Ω for samples N-ReS_2-2/CC, N-ReS_2-4/CC, and N-ReS_2-8/CC, respectively. It proves that N-implanting effectively improves the electronic conductivity of the ReS_2-based electrocatalyst.

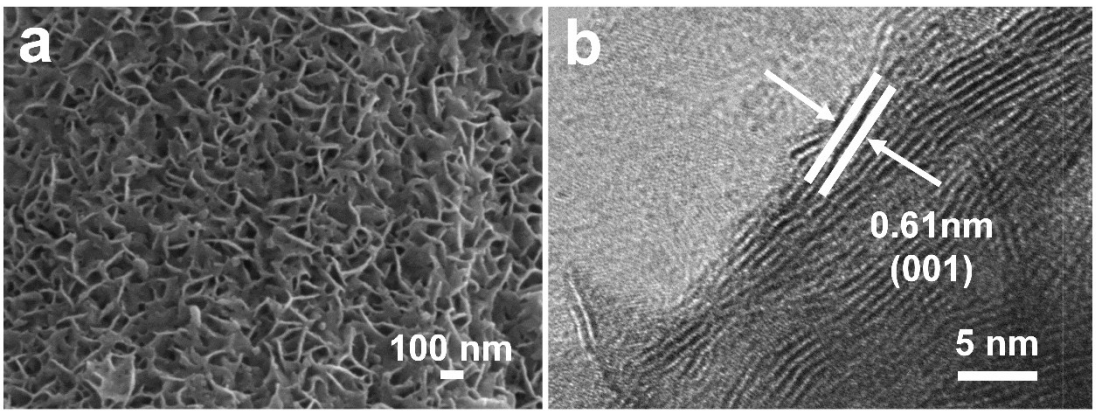

Fig. S9. (a) SEM and (b) HRTEM images of the N-ReS_2-6/CC after 140h stability test.

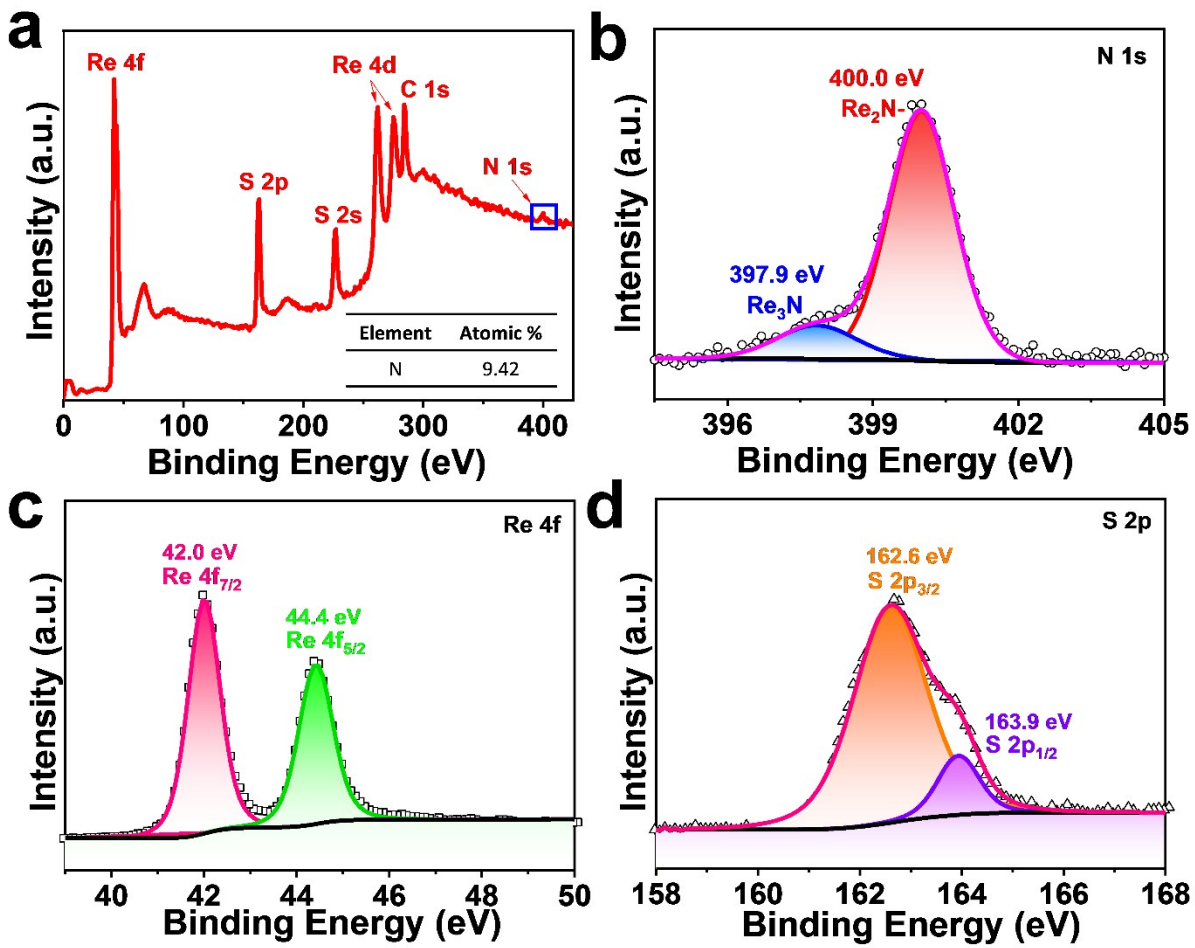

Fig. S10. XPS spectra of (a) survey spectra, (b) N 1s, (c) Re 4f and (d) S 2p for N-ReS_2-6/CC after 140h stability test.

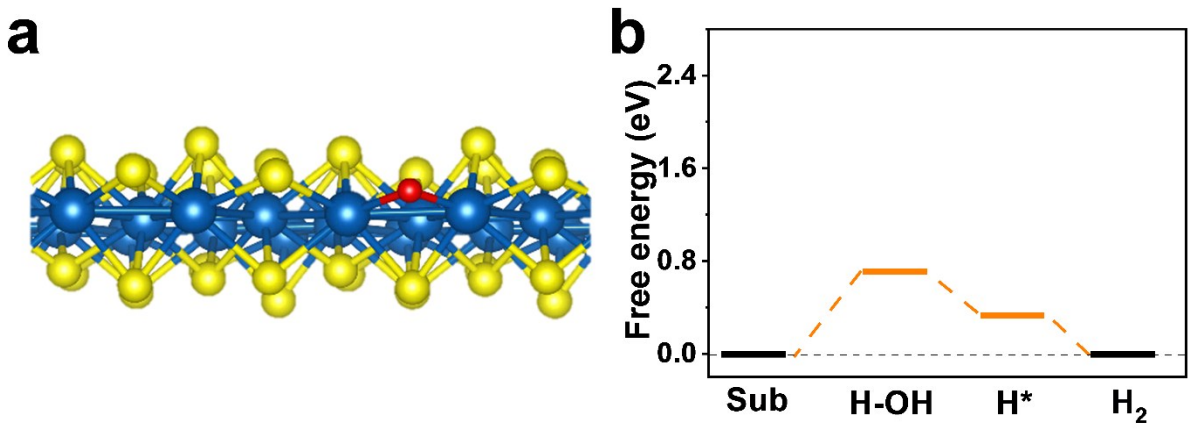

Fig. S11. (a) Simulated models of high-site e-N-ReS_2. (b) The calculated free energy diagram of high-site e-N-ReS_2.

Because of the highly asymmetric structure of the 1T'-phase ReS_2, there are two possible ways of replacing the edge S atom to form N-implanting site,[2] i.e., the low-site e-N-ReS_2 and high-site e-N-ReS_2. For high-site e-N-ReS_2, the values of ΔG_{H2O} and ΔG_{H*} are 0.712 eV and 0.332 eV (**Fig. S11b**). Compared with the e-ReS_2, the values of ΔG_{H*} and ΔG_{H2O} of high-site e-N-ReS_2 and low-site e-N-ReS_2 have the same downward trend. This result indicates that the N-implanting (no matter at high-site or low-site) could improve the HER activity. On the other hand, the formation energy of high-site e-N-ReS_2 (0.131 eV) and low-site e-N-ReS_2 (0.111 eV) has nearly equal values (**Table S3**). This indicates that they have similar thermodynamic stability and both cases could be occurred during the N-implanting process. Therefore, in the main article, we use the low-site e-N-ReS_2 as an example to illustrate.

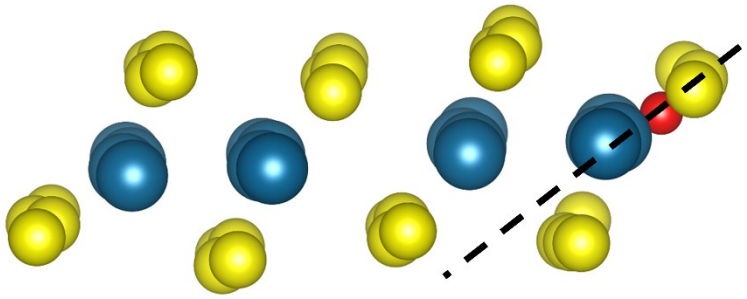

Fig. S12. The side view of e-N-ReS_2. The inset cross section denotes the plane used to calculate the difference charge density in **Fig. 5d**.

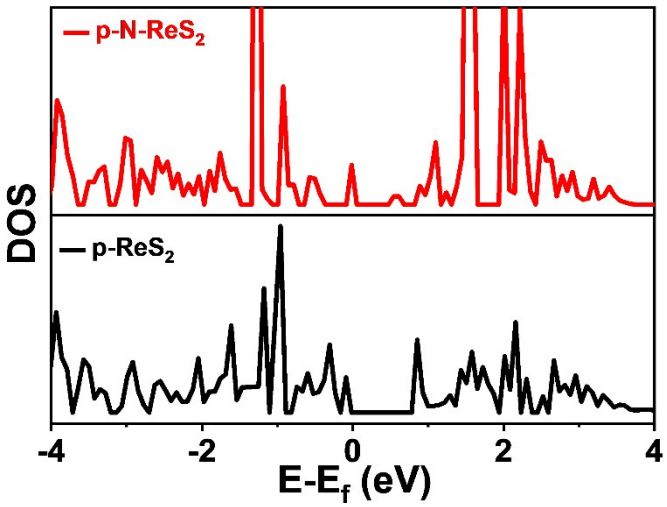

Fig. S13. DOS plots of p-ReS_2 (black line) and p-N-ReS_2 (red line).

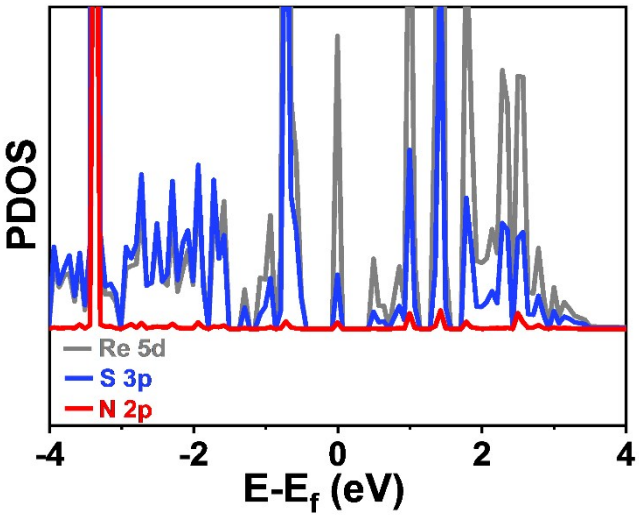

Fig. S14. The PDOS plots of Re 5d (grey line), S 3p (blue line) and N 2p (red line) orbitals for e-N-ReS_2.

Table S1. The atomic percentage of N (at. %) was determined by XPS.

Samples	Atomic percentage N (at. %)
N-ReS_2-2/CC	7.68
N-ReS_2-4/CC	8.42
N-ReS_2-6/CC	9.67
N-ReS_2-8/CC	9.69

The molar ratio between NH_4ReO_4 and CH_4N_2S in the precursor increased from 1:2 to 1:6, the N contents were increased obviously. When the ratio increases to 1:8, the content of N in the sample after reaction is essentially unchanged, indicating that implanting has reached a saturation point.

Table S2. Comparison of HER activity with that of previously reported TMD electrocatalysts.

Samples	Overpotential at 10 mA cm^{-2} (mV)	Tafel ($mV\ dec^{-1}$)	Electrolyte	References
N-ReS_2-6/CC	**90**	**85**	**1 M KOH**	**This work**
ReS_2/Ni_3S_2	168	118	1 M KOH	[3]
SWCNTs/c-ReS_2	327	-	1 M KOH	[4]
Fe-ReS_2@N-CNF	≈ 240	63	0.1 M Na_2SO_4	[5]
ReS_2 on 3D-printed carbon electrodes	383	103	0.5 M H_2SO_4	[6]
Monolayer ReS_2 with Re defect	147	69	0.5 M H_2SO_4	[7]
ReS_2/carbon fibre clothes	170	146	0.5 M H_2SO_4	[8]
F-CoS_2@NF	112	61	1 M KOH	[9]
CoO@1T-MoS_2	117	84	1 M KOH	[10]
V-MoS_2	206	97	1 M KOH	[11]
P-MoS_2	226	144	1 M KOH	[12]
$MoS_2/MoSe_2$	235	96	1 M KOH	[13]
Co_9S_8@MoS_2	177	84	1 M KOH	[14]
$MoSe_2/SnS_2$	285	109	1 M KOH	[15]
Co-MoS_2/Mo_2CT_x MXene	112	82	1 M KOH	[16]

Table S3. The formation energy of two types of N-implanting into the edge sites.

Different structures	Low-site e-N-ReS_2	High-site e-N-ReS_2
Formation energy (eV)	0.131	0.111

Table S4. The Gibbs free energy of hydrogen adsorption (ΔG_{H*}) on different sites for p-ReS_2 and p-N-ReS_2.

Sites for H adsorption	p-ReS_2 (ΔG_{H*}/eV)	p-N-ReS_2 (ΔG_{H*}/eV)
1	1.280	0.686
2	1.303	0.744
3	1.452	0.830
4	1.801	1.393
5	1.562	1.236
6(N)	1.793	-1.093

Table S5. The Gibbs free energy of hydrogen adsorption (ΔG_{H*}) on different sites for e-ReS_2, low-site e-N-ReS_2, and high-site e-N-ReS_2.

Sites for H adsorption	e-ReS_2 (ΔG_{H*}/eV)	Low-site e-N-ReS_2 (ΔG_{H*}/eV)	High-site e-N-ReS_2 (ΔG_{H*}/eV)
1	0.786	0.082	0.332
2 (Low-site N)	0.390	-1.488	-0.345
3 (High-site N)	0.791	0.347	-1.574
4	0.391	-0.293	-0.341
5	1.561	0.841	1.415
6	1.461	0.141	0.770
7	1.562	0.903	0.729
8	1.462	0.943	0.443

Table S6. The corresponding ΔG_{H^*} calculated from the models with different amounts of N-implanting in e-ReS_2.

Models	ΔG_{H^*} (eV)
e-ReS_2	0.390
e-N-ReS_2	0.082
e-2N-ReS_2	-0.073
e-3N-ReS_2	0.094

In order to investigate the effect of the concentration of N-implanting on the H adsorption/desorption at edge S sites, the ΔG_{H^*} of models with various amounts of N-implanting were further calculated. The models with one, two and three S atoms replaced by N atoms were named as e-N-ReS_2, e-2N-ReS_2, and e-3N-ReS_2, respectively. With the increase of N-implanting, the absolute value of ΔG_{H^*} showed a trend of first decreasing and then increasing. The ΔG_{H^*} value of e-2N-ReS_2 is -0.073 eV, which is much closer to zero than those of e-N-ReS_2 (0.082 eV) and e-3N-ReS_2 (0.094 eV). These results clearly demonstrate that N-implanting is an effective way to modulate the H adsorption/desorption during HER over ReS_2.

Table S7. The correlation of ΔG_{H^*} with electron amount transfer from S to H, which characterizes e-ReS_2 and e-N-ReS_2 to catalyze (H^++e^-) pair.

Samples	Amount of electron transferred from S to H (a. u.)	ΔG_{H^*} (eV)
e-ReS_2	0.912	0.786
e-N-ReS_2	0.968	0.082

References:

[1] K. Sun, L. Zeng, S. Liu, L. Zhao, H. Zhu, J. Zhao, Z. Liu, D. Cao, Y. Hou, Y. Liu, Y. Pan and C. Liu, *Nano Energy*, 2019, **58**, 862-869.

[2] Z. Lai, A. Chaturvedi, Y. Wang, T. H. Tran, X. Liu, C. Tan, Z. Luo, B. Chen, Y. Huang, G. H. Nam, Z. Zhang, Y. Chen, Z. Hu, B. Li, S. Xi, Q. Zhang, Y. Zong, L. Gu, C. Kloc, Y. Du and H. Zhang, *J. Am. Chem. Soc.*, 2018, **140**, 8563-8568.

[3] X. Lu, R. Liu, Q. Wang and C. Xu, *ACS Appl. Mater. Interfaces*, 2019, **11**, 40014-40021.

[4] B. Martin-Garcia, D. Spirito, S. Bellani, M. Prato, V. Romano, A. Polovitsyn, R. Brescia, R. Oropesa-Nunez, L. Najafi, A. Ansaldo, G. D'Angelo, V. Pellegrini, R. Krahne, I. Moreels and F. Bonaccorso, *Small*, 2019, 1904670.

[5] F. Lai, N. Chen, X. Ye, G. He, W. Zong, K. B. Holt, B. Pan, I. P. Parkin, T. Liu and R. Chen, *Adv. Funct. Mater.*, 2020, 1907376.

[6] S. Ng, C. Iffelsberger, Z. Sofer and M. Pumera, *Adv. Funct. Mater.*, 2020, 1910193.

[7] Y. Zhou, E. Song, J. Zhou, J. Lin, R. Ma, Y. Wang, W. Qiu, R. Shen, K. Suenaga, Q. Liu, J. Wang, Z. Liu and J. Liu, *ACS Nano*, 2018, **12**, 4486-4493.

[8] X. Xu, H. Zhao, R. Wang, Z. Zhang, X. Dong, J. Pan, J. Hu and H. Zeng, *Nano Energy*, 2018, **48**, 337-344.

[9] L. Lei, D. Huang, C. Zhang, R. Deng, S. Chen and Z. Li, *J. Catal.*, 2020, **385**, 129-139.

[10] Y. Huang, Y. Sun, X. Zheng, T. Aoki, B. Pattengale, J. Huang, X. He, W. Bian, S. Younan, N. Williams, J. Hu, J. Ge, N. Pu, X. Yan, X. Pan, L. Zhang, Y. Wei and J. Gu, *Nat. Commun.*, 2019, **10**, 982.

[11] S. Bolar, S. Shit, J. S. Kumar, N. C. Murmu, R. S. Ganesh, H. Inokawa and T. Kuila, *Appl. Catal. B Environ.*, 2019, **254**, 432-442.

[12] P. Vishnoi, K. Pramoda, U. Gupta, M. Chhetri, R. G. Balakrishna and C. N. R. Rao, *ACS Appl. Mater. Interfaces*, 2019, **11**, 27780-27787.

[13] Q. Zhou, G. Zhao, K. Rui, Y. Chen, X. Xu, S. X. Dou and W. Sun, *Nanoscale*, 2019, **11**, 717-724.

[14] L. Diao, B. Zhang, Q. Sun, N. Wang, N. Zhao, C. Shi, E. Liu and C. He, *Nanoscale*, 2019, **11**, 21479-21486.

[15] Y. Chen, X. Wang, M. Lao, K. Rui, X. Zheng, H. Yu, J. Ma, S. X. Dou and W. Sun, *Nano Energy*, 2019, **64**, 103918.

[16] J. Liang, C. Ding, J. Liu, T. Chen, W. Peng, Y. Li, F. Zhang and X. Fan, *Nanoscale*, 2019, **11**, 10992-11000.